What caused the interdecadal shift of the ENSO impact on dust mass concentration over northwestern South Asia？

Lamei Shi [1,2], Jiahua Zhang [1,2], Da Zhang [1,2], Jingwen Wang [1,2], Xianglei Meng[2], Yuqin Liu[3], Fengmei Yao [2]

[1] Key Laboratory of Digital Earth Science, Aerospace Information Research Institute, Chinese Academy of Sciences, Beijing 100094, China

[2] College of Earth and Planetary Sciences, University of Chinese Academy of Sciences, Beijing 101407, China

[3] Key Laboratory of Urban Environment and Health, Institute of Urban Environment, Chinese Academy of Sciences, Xiamen 361021, China

Correspondence to: Jiahua Zhang (zhangjh@radi.ac.cn)

Abstract. The changes of large-scale circulation, especially El Niño-Southern Oscillation (ENSO), have significant impacts on dust activities over the dust source and downwind regions. However, these impacts present an interdecadal pattern and it remains less clear that which factors lead to the interdecadal variability of the ENSO impact on dust activities over the northwestern South Asia, although previous studies have discussed the response of the interannual dust activities over the northwestern South Asia to the ENSO circle. Based on the linear regression model and MERRA-2 atmospheric aerosol reanalysis data, this study investigated the interdecadal variability of the ENSO impact on dust activities as well as the associated possible atmospheric drivers under two different warming phases over the northwestern South Asia. Results indicated that the relationship between ENSO and Dust Column Mass Density (DUCMASS) experienced an obvious shift from the accelerated global warming period (1982–1996) to the warming hiatus period (2000–2014). The change of Atlantic and Indian ocean SSTA pattern weakened the impact of ENSO on dust activities over the northwestern South Asia during 1982–1996, while the change of PDO strengthened ENSO's effect when it was in phase with ENSO. Both the Atlantic and Indian Ocean SSTA patterns were modulated by the duration of ENSO events (i.e., continuing and emerging ENSO). This study provides new sights to numerical simulation involving the influence of atmospheric teleconnections on the variability of dust activities and their influence mechanisms.

Keywords: Surface dust mass concentration; ENSO–DUCMASS relationship; interdecadal change; large-scale atmospheric circulation; northwestern South Asia

1 Introduction

Dust aerosol is attracting an increasing concern due to its adverse impacts on human health (Bozlaker et al., 2013; Chen et al., 2004; Erel et al., 2006; Kaiser and Granmar, 2005; Poulsen et al., 1995; Sanchez de la Campa et al., 2013; Schulz et al., 2012) and environmental problems (Avila, 1998; Behrooz et al., 2017; Razakov and Kosnazarov, 1996). The Northwest Indian subcontinent, which is the most arid and semiarid area of South Asia, suffers heavy and frequent dust storms in summer due to extremely dry climate and strong winds (Jin and Wang, 2018). Those dust can travel long-distance to North India and the Arabian Sea, degrading air quality (Mahowald et al., 2010) and modifying ocean biogeochemistry processes (Richon et al., 2018; Singh et al., 2008). Particularly, dust aerosols can change local radiation budget, circulations, and Indian summer monsoon rainfall through absorption and scattering of solar radiation. The mineral dust over the northwestern South Asia is closely associated with the long-term variation of global climate (Banerjee et al., 2019; Bollasina et al., 2011; Jin et al., 2018). To better understand such feedback, and give early warning to reduce disasters and losses caused by dust events, it is important to find out the controlling factors of the Dust Column Mass Density (DUCMASS) and its long-term variation.

ENSO, as a periodic fluctuation in sea surface temperature (SST) and the air pressure across the equatorial Pacific Ocean, is as the primary large-scale driver of dust loading over the global dust source region (Trenberth et al., 2014). Prospero and Nees (1986) found that ENSO-related large-scale atmospheric circulation changes led to the increase in winter dust concentration over North Africa. Xi and Sokolik (2016a) indicated that in La Niña years, the precipitation and soil moisture over Central Asia decreased and caused poor vegetation conditions and heavy drought conditions, which strengthened dust activities. Yu et al. (2015b) suggested that La Niña events provided favorable conditions for dust activities over Saudi Arabia. However, Banerjee et al. (2016) proposed that the low-level southwesterly winds and high-level westerly winds accompanied with La Niña events were the main factor that contributed to the elevated dust levels over the Arabia Peninsula. Abish and Mohanakumar (2013) pointed out that strengthened westerly circulation related with El Niño increased the dust transmission from the Middle East to the Indian subcontinent. Simultaneously, the impacts of ENSO on dust activities were also modulated by other atmospheric factors, e.g., PDO could strengthen the effect of ENSO when

58   it was in phase with ENSO (He et al., 2013; Wang et al., 2008; Wang et al., 2014); the spring dust index

59   over the northern China in the years when negative AO and El Niño occurred synchronously was

60   significantly higher than that in the years when positive AO and La Niña were concurrent (Liu et al.,

61   2020; Lee et al., 2015); IOD could also influence the dust activities over the northwestern Indian ocean

62   by adjusting the El Niño related water vapor conditions (Banerjee and Kumar, 2016).

63   ENSO exhibits profound impacts on the global climate. Nevertheless, the Earth climate is varying

64   and ENSO, including its feedback and influences on the changing global climate, also experience

65   significant changes (Ashok et al., 2007; Weare et al., 1976; Weng et al., 2007; Yang and Jiang, 2014; Yu

66   and Kao, 2007; Yuan and Yang, 2012). In the mid-1970s, an interdecadal climate regime shift was

67   observed in the large-scale boreal winter circulation pattern over the North Pacific (Graham, 1994; Nitta

68   and Yamada, 1989; Trenberth and Hurrell, 1994). Another remarkable climate change was observed in

69   the early 21st century, i.e., an accelerated global warming prevailed before late 1990s and a warming

70   hiatus dominated after that (Easterling and Wehner, 2009; Fyfe et al., 2011, 2013). After 2013, the global

71   warming hiatus came to an end due to a persistent warm condition over the equatorial Pacific between

72   Mar. 2014 and May 2016 (Hu and Fedorov, 2017). Concurrent with the Pacific climate shift, the large-

73   scale circulation pattern and their atmospheric teleconnection also exhibited an interdecadal change, e.g.,

74   the correlation between El Niño and rainfall over India turned to be insignificant from the late 1970s,

75   simultaneously, the relationship between ENSO and monsoon also weakened around this turning point

76   (Kumar et al., 1999). Two influence mechanisms were proposed to explain this weakened ENSO–

77   monsoon relationship. One was the varied location of Walker circulation that adjusted the monsoon

78   rainfall over Indian region, the other was the temperature change over Eurasia that modulated the land-

79   sea thermal gradient. Besides, the impact of Atlantic Ocean pattern on the monsoon circulation over the

80   Indian Ocean became stronger since late 1970s as the influence of the tropical Pacific has reduced

81   (Kucharski et al., 2007; Sabeerali et al., 2019; Srivastava et al., 2019). This in-turn impacted the

82   circulation responsible for dust uplift and transport.

83   It was reported that the effect of ENSO on Indian summer monsoon rainfall (ISMR), which was an

84   important modulator to DUCMASS, experienced a remarkable interdecadal change and many factors

85   may cause this transition (Yang and Huang, 2021). Till now, the interdecadal variability in the links of

86 DUCMASS over the northwestern South Asia with ENSO has not been fully investigated, as compared

87 to the North African and West Asian counterpart (Yu et al., 2015). In addition, though many factors have

88 been proved to influence the short-term (e.g., interannual scale) variation of the relationship between

89 ENSO and dust activities over South Asia, their effects on the long-term (e.g., interdecadal scale) change

90 are still unclear. Cai et al. (2014) pointed out that global warming will have a significant impact on ENSO.

91 The extreme El Niño events will become more frequent under the changes of atmospheric convention in

92 the next half of the 21st century. Thus, understanding the physical mechanism of the shifting ENSO–

93 DUCMASS relationship is of profound implications for the forecast of dust trend in the future climate

94 change scenario. This study aims to investigate the large-scale atmospheric factors that contribute to the

95 interdecadal variability of the ENSO impact on DUCMASS over the northwestern South Asia.

96 The paper is organized in the following structure: section 2 describes the datasets and methods;

97 section 3 presents factors that influence the interdecadal change of the relationship between DUCMASS

98 and wintertime Niño-3 index; section 4 discusses the deficiency and prospect of this study, and the

99 conclusions are given in section 5.

100 **2 Data and methods**

101 **2.1 Study area**

102 The main dust source over South Asia is a large arid region in the northwestern part of the Indian

103 subcontinent, which stretches from India to Pakistan. Most of the dust aerosols over this region come

104 from the Thar desert. The southeastern part of the Thar desert lies between the Aravalli Hills. The desert

105 extends as far as the Punjab Plain in the north and northeast, the alluvial plains of the Indus River in the

106 west and northwest, and the Great Rann of Kutch along the western coast. The desert presents an

107 undulating surface, with high and low sand dunes separated by sandy plains and low barren hills. The

108 soils are mainly consisted by desert soils, red desertic soils, sierozems, the red and yellow soils of the

109 foothills, the saline soils of the depressions, and the lithosols (shallow weathered soils) and regosols (soft

110 loose soils) found in the hills. The subtropical desert climate here results from persistent high pressure

111 and subsidence. The prevailing southwest monsoon winds from Indian Ocean that bring rain to much of

112 the Indian subcontinent in summer tend to bypass the Thar to the east. The soils are generally infertile

113 and overblown with sand due to severe wind erosion (Augustyn et al., 2019). The amount of annual

114 rainfall in the desert is low, ranging from about 100 mm or less in the west to about 500 mm in the east.

115 Almost 90 % of the annual rainfall occurs in the season southwest monsoon, from July to September.

116 While the prevailing wind is dry northeast monsoon during other seasons. Dust storms and dust-raising

117 winds are common from May to July (Chauhan, 2003). Thus, the DUCMASS used in this study is

118 averaged from June to July and May is neglected to eliminate the disturbance of seasonal climatological

119 differences. Analysis is carried out over the dust source in the northwestern South Asia (65°–82° E, 24°–

120 32° N), as shown in Fig. 1. All variables involving spatial average are taken from this region unless stated

121 otherwise.
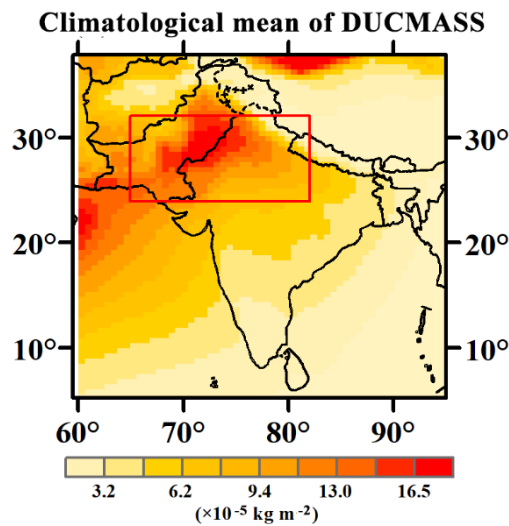
122
123 **Figure 1: Climatological mean DUCMASS over South Asia based on the MERRA-2 dataset. The dust source**
124 **over the northwestern South Asia is marked with red rectangle.**

125 **2.2 Datasets**

126 **2.2.1 Dust concentration**

127   Dust column mass density from 1982 to 2014 was obtained from the Modern-Era Retrospective

128 Analysis for Research and Applications, version 2 (MERRA-2). MERRA-2 is produced via the Goddard

129 Earth Observing System-Data Assimilation System (GEOS-DAS, version 5.12.4) based on GEOS-5

130 climate model and the Gridpoint Statistical Interpolation (GSI) analysis scheme (Gelaro et al., 2017).

131 Extensive satellite data are integrated into MERRA-2 to estimate dust concentration (Randles et al., 2017;

132 Veselovskii et al., 2018). The dust products were comprehensively validated using the results of ground-

133 based observation, satellite measurements, and numerical simulation (Buchard et al., 2017; Randles et

al., 2017). They have been widely applied to researches on global environment and climate change (He et al., 2019; Randles et al., 2017). The variable "Dust Column Mass Density-PM$_{2.5}$" (DUCMASS25) with a spatial resolution of 0.625°×0.5° (longitude×latitude) used in this study is from the dataset of "tavgM_2d_aer_Nx".

2.2.2 Land and sea surface temperature

To explore the possible influence of SST on the South Asian dust activity, we used three SST datasets from 1981 to 2014 for comparison: (1) The National Oceanic and Atmospheric Administration (NOAA) Extended Reconstructed SST (ERSST) version 5 (Huang et al., 2017) that is available at 2°×2° spatial resolution is used for analysis, (2) Centennial in situ Observation-Based Estimates (COBE) version 2 SST data at 1°×1° spatial resolution (Hirahara et al., 2014) and (3) Hadley Centre Global Sea Ice and Sea Surface Temperature (HadISST1.1) dataset produced by the Met Office, starting from 1870 up to the present with a horizontal resolution of 1°×1° (Rayner et al., 2003). While the land-sea thermal contrast was calculated from the Hadley Centre Climate Research Unit Temperature version 5.0.1.0 (HadCRUT5) data from 1981 to 2014, which is a blend of the Climatic Research Unit land-surface air temperature dataset (CRUTEM5) and the Hadley Centre sea-surface temperature (HadSST4) dataset (Osborn et al., 2021). The longitude and latitude of SST index involved in this study were shown in Table 1.

Table 1: Longitude and latitude of SST index used in this study.

Acronyms	Full Name	Longitude and Latitude	Involved Ocean
Niño-3	——	150°–90° W, 5° S–5° N	Pacific
Niño-3.4	——	170°–120° W, 5° S–5° N	Pacific
Niño-4	——	160° E–150° W, 5° S–5° N	Pacific
ASGI	Atlantic SSTA gradient index	North: 60°–30° W, 0–20° N South: 20° W–10° E, 0–20° S	Atlantic Ocean
TWISSTA	Tropical western Indian ocean SSTA	50°–70° E, 10° S–15° N	Indian Ocean
IOD	Indian Ocean Dipole	West: 50°–70° E, 10° S–10° N East: 90°–110° E, 10° S–0°	Indian Ocean

| PDO | Pacific decadal oscillation | 117.5° E–77° W, 20°–66.5° N | Pacific |

2.2.3 Large-scale climate indices

Three monthly Niño indices Niño-3, Niño-3.4, and Niño-4 from 1981 to 2014, which monitor the SST anomalies averaged across the eastern equatorial Pacific, Pacific from dateline to the South American coast, and central equatorial Pacific, respectively, were used to analyze their links with DUCMASS over the northwestern South Asia. Kinter et al. (2002) pointed out that Nov.–Jan. is the peak season for El Niño/La Niña, thus the average Niño index from (–1) Nov. to (0) Jan. was used. Only one Niño index that showed the highest correlation coefficient was retained in this study, i.e., Niño-3. The time series of ENSO was represented by Niño-3 and Niño-3 also referred to ENSO. The large-scale climate indices, such as PDO and IOD, was also used to explore the potential factors that contributed to the interdecadal shift of ENSO–DUCMASS relationship. All those indices were from the Climate Predict Center of National Oceanic and Atmospheric Administration (NOAA/CPC).

2.3 Method

In this study, we compared the impact of ENSO on DUCMASS over the northwestern South Asia under two different warming epochs, and investigated the potential global change drivers to the shift of ENSO–DUCMASS relationship. The global warming was separated into the accelerated warming period from 1982 to 1996 (P1) and the warming hiatus period from 2000 to 2014 (P2). The year 2014 was added to the warming hiatus period to keep the length of those two periods consistent. This classification was not controversial since the ENSO year stated in this study spanned from antecedent November to current January.

2.3.1 Contribution of factors to relationship

The contribution of X (Indian Ocean SSTA, Atlantic SSTA gradient index, and PDO) modifying ENSO–DUCMASS relationship was defined as: sliding regression of X onto Niño-3 index multiplies by sliding regression of DUCMASS onto X with Niño-3 removed (Yang and Huang, 2021).

2.3.2 Signal removal method

The ENSO signals were removed from the oceanic SSTA pattern when analyzing spatial coupling

177 and regression mode between the oceanic SSTA pattern and DUCMASS as well as local surface

178 conditions (precipitation, soil moisture, land cover, wind, etc). Simultaneously, the oceanic SSTA signals

179 were removed from ENSO when calculating the sliding correlation between ENSO and DUCMASS. In

180 this study, the residual time series based on the linear regression method were used to represent the ENSO

181 (or oceanic SSTA index)-independent components (Yang and Huang, 2021), as shown in Eq. (1):

$$\xi_{remove} = \xi - Z \times \frac{cov(\xi, Z)}{var(Z)} \tag{1}$$

182 Where ξ_{remove} is the time series of variable ξ with Z removed, ξ is the time series of original

183 variable, Z is the time series of related signal that needs to be removed, cov indicates the covariance

184 between two variables, and var indicates the variance of ENSO.

185 **2.3.3 Coupled spatial pattern analysis**

186 The maximum covariance analysis (MCA) is a useful tool for isolating the most coherent pairs of

187 spatial patterns and their associated time series by performing an eigenanalysis on the temporal

188 covariance matrix between two geophysical fields (Storch and Zwiers, 1999). The MCA method was

189 used to analyze the coupled patterns between DUCMASS and oceanic SSTA.

190 **2.3.4 Definition of different types of ENSO**

191 Following Yang and Huang (2021), the EM and CT ENSO were defined based on the three-month

192 running mean of the Niño-3 index. Two situations for the CT ENSO were considered, i.e., the slowly

193 decaying events and the developing events since the previous winter. For the slowly decaying situation,

194 a CT ENSO was identified when the average Niño-3 of (–1) Oct.–(0) Jan. was greater than 0.5 (below –

195 0.5) standard deviation (STD), became greater than 0.5 (below –0.5) STD in single month during (0)

196 Mar.–(0) May, and remained positive (negative) during (0) Jun.–(0) Sep.. For the developing events since

197 the previous winter, a CT ENSO was identified when the Niño-3 was greater than 0.75 (below –0.75)

198 STD in any month from (–1) Oct. to (0) May, accompanied by positive (negative) values for eight single

199 months, and the average Niño-3 of (0) Jun.–(0) Sep. was greater than 0.5 (below –0.5) STD. To acquire

200 more available samples in the study period, all the ENSO years that were not defined as CT ENSO were

201 identified as EM ENSO year in this study, which was different from Yang and Huang (2021). Based on

202 this definition, the CT El Niño years during 1982–2014 included 1982, 1983 and 1987; CT La Niña years

203   included 1984, 1985, 1989, 1996, 1999, 2000, and 2011; EM El Niño years included 1995, 1998, 2003,

204   2005, 2007, and 2010; EM La Niña years included 2008 and 2012.

205   In this study, "(0) month" represented the year concurrent with the year when DUCMASS was

206   acquired and "(–1) month" represented the preceding year.

207   **3 Results**

208   **3.1 Observed interdecadal change of the impact of ENSO on DUCMASS**

209   In the present study, we found that the DUCMASS–Niño-3 relationship experienced an interdecadal

210   transition at around 1999/2000. Based on the 15-year sliding correlation from 1982 to 2014 (Fig. 4 (a)),

211   the DUCMASS–Niño-3 relationship was weak before the early of 2000s and became stronger after that.

212   Specifically, the winter Niño-3 index ((–1) Nov.–(0) Jan.) presented a significant negative relation (R=–

213   0.68, p<0.01) with DUCMASS during 2000–2014 (P2), while no significant correlation (R=–0.41,

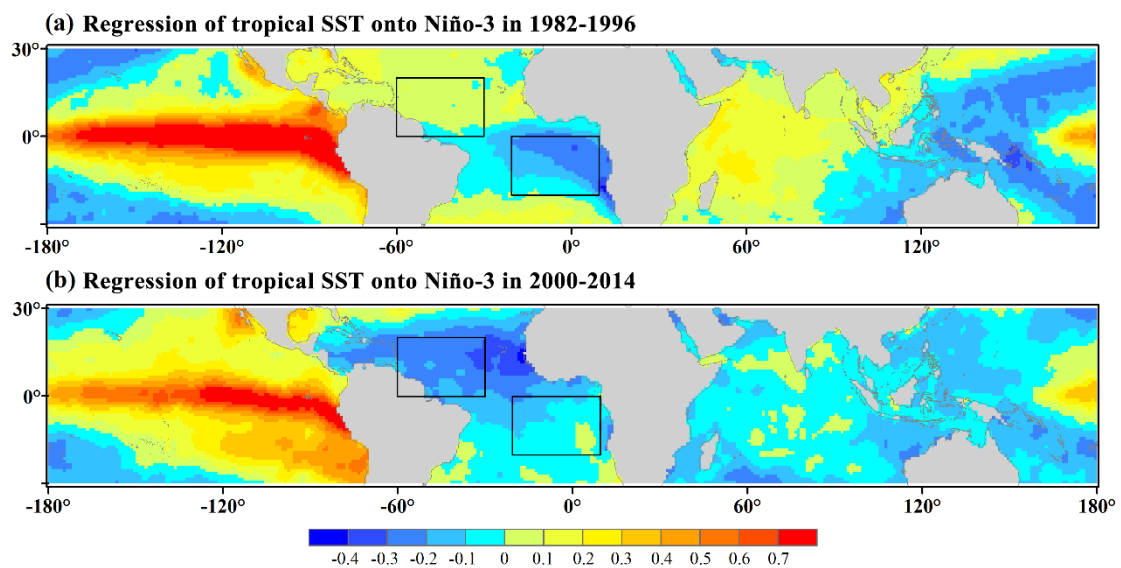214   p>0.05) was observed in 1982–1996 (P1), as shown in Fig. 2.
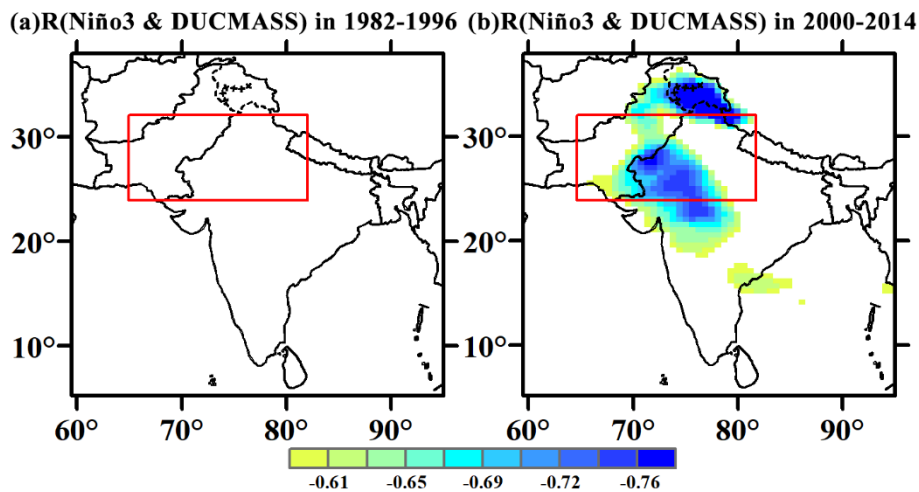
215

216   **Figure 2: Correlation between Niño-3 index and DUCMASS over South Asia during (a) 1982–1996 and (b)**

217   **2000–2014. (Only correlations that passed the 99% confidence level were presented).**

218   **3.2 Factors influencing the interdecadal change of the impact of ENSO on DUCMASS**

219   **3.2.1 Tropical Atlantic SSTA pattern**

220   With the global climate change observed in early 2000s, the ENSO-related tropical Atlantic SSTA

221   experienced an obvious transition, i.e., from an Atlantic Niña pattern during 1982–1996 to an Atlantic

222   Niño pattern during 2000–2014 (Fig. 3), which coincides with the findings of Yang and Huang (2021).

223   The tropical Atlantic SSTA pattern was a crucial factor for the restoration of ENSO–ISMR relationship

224   since the late 1990s (Yang and Huang, 2021), thus, it could also disturb the impact of ENSO on dust

225   activities over the northwestern South Asia. In order to validate the connection between the Atlantic

226   SSTA and the DUCMASS–Niño-3 relationship, an Atlantic SSTA gradient index (ASGI) was used to

227   describe the SSTA pattern shift in the tropical Atlantic, which represented the difference of averaged

228   SSTA between tropical North Atlantic and tropical South Atlantic (marked by two rectangles in Fig. 3).

229   According to Tokinaga et al. (2019), the Atlantic Niña pattern develops and is most sensitive to ENSO

230   in spring, thus the SST averaged from Mar. to May was used in this section.

(a) Regression of tropical SST onto Niño-3 in 1982-1996

**(b) Regression of tropical SST onto Niño-3 in 2000-2014**

231

232   **Figure 3: Regression of spring (Mar.–May) tropical SSTA onto Niño-3 index. Black rectangles denote the**
233   **regions to define ASGI. The range of the upper one is 60–30° W, 0–20° N and that of the lower one is 20° W–**
234   **10° E, 20–0° S. (Similar with Fig. 2 (c)–(d) of Yang and Huang (2021) but with different time spans)**

235   The relationship between Niño-3 and DUCMASS witnessed a reversal at the early 2000s,

236   simultaneously, the correlation between Niño-3 and ASGI exhibited the similar change. The correlation

237   between Niño-3 and ASGI passed the 99% confidence level during P1, while it did not pass the 95%

238   confidence level during P2, as shown in Fig. 4 (b). However, the correlation between Niño-3 and

239   DUCMASS showed a contrary trend with a higher correlation coefficient appeared in P2. Figure 4 (a)

240   showed that the DUCMASS–Niño-3 relationship was weakened when the ASGI signals were removed

241   from Niño-3 index during P1, while during P2, the DUCMASS–Niño-3 relationship remained the same

242   with or without the ASGI signals removed. In addition, the contribution of ASGI to the DUCMASS–

243   Niño-3 relationship (Fig. 4 (c)) proved that during P1, ASGI weakened this relationship while no

significant contribution was observed during P2. Thus, it is hypothesized that the strengthening (weakening) of the response of ASGI to Niño-3 weakened (strengthened) the impact of Niño-3 on DUCMASS during P1 (P2).
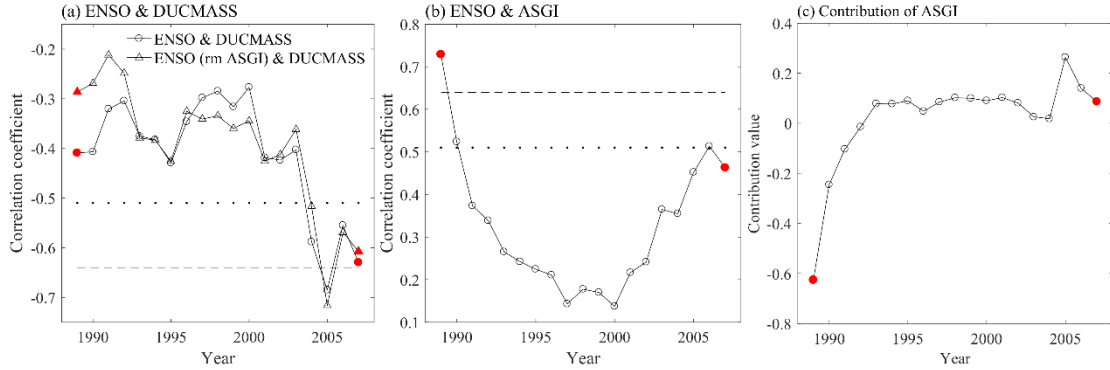

Figure 4: (a) The 15-year sliding correlation between DUCMASS and Niño-3 with and without ASGI-related signals removed; (b) 15-year sliding correlation between Niño-3 and ASGI; (c) Sliding contribution of ASGI to DUCMASS–Niño-3 relationship. The two red filled markers represented the 15-year window spanning from 1982 to 1996 and 2000 to 2014, respectively. The x-axis denotes the middle year of the period under analysis.
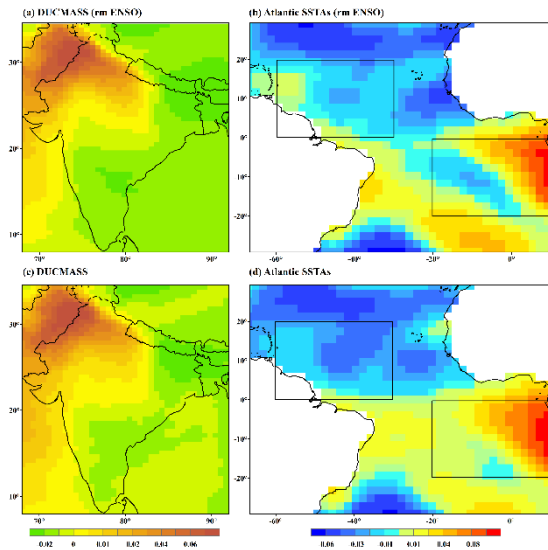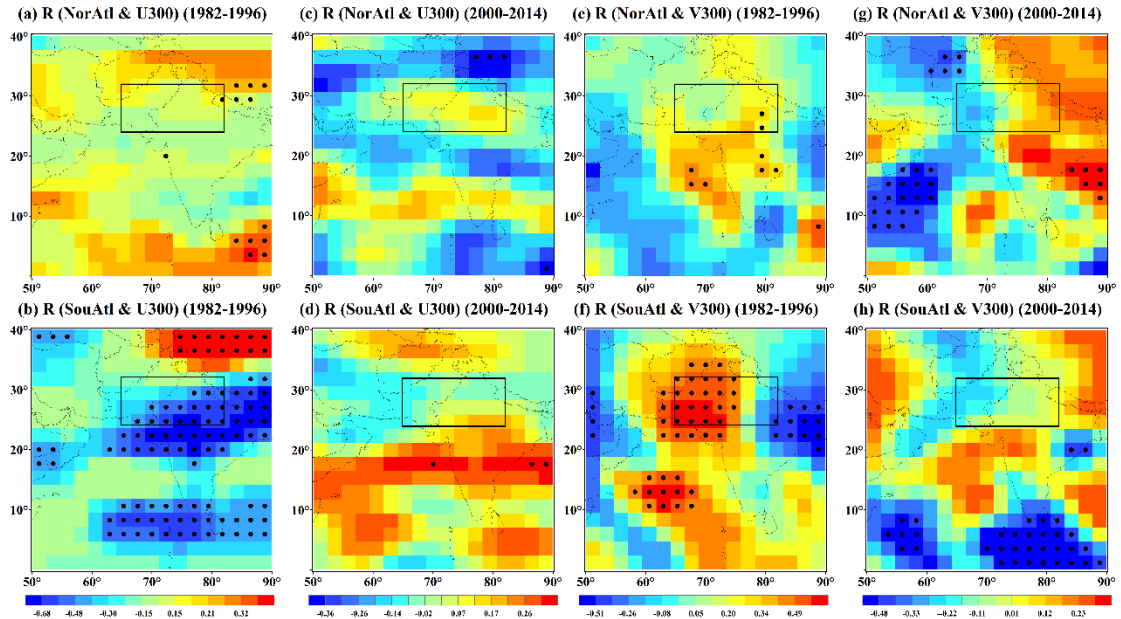

Figure 5: Spatial correlation between spring (Mar.–May) tropical Atlantic SSTA and DUCMASS of the first mode of the MCA analysis in 1982–2014. The first MCA mode of (a) the DUCMASS, and (b) the tropical Atlantic SSTA with ENSO-related signals removed. (c)–(d) As in (a)–(b), but for the original series including the ENSO signal.

In order to validate the effect of Atlantic SSTA pattern on the DUCMASS–Niño-3 relationship, the spatial coupling mode between DUCMASS and tropical Atlantic SSTA was explored. Figure 5 showed that the negative ASGI, i.e., negative SST anomaly over the tropical North Atlantic and positive SST anomaly over the tropical South Atlantic, was coupled with increased DUCMASS over the northern and

northwestern India. This pattern was not impacted by ENSO since the MCA results with ENSO-related

signals removed were similar with that including the ENSO-related signals, as shown in Fig. 5. Figures

6 and 7 further illustrated the influence mechanism of Atlantic SSTA pattern onto DUCMASS. Figure 6

showed that the effect of North and South Atlantic SSTA (NorAtl/SouAtl) with ENSO signal removed

on the geopotential height (GP) at 850hPa/300hPa exhibited significant difference during P1, while they

were close (all are not significant) in P2. Similarly, significant difference was also seen in the effect of

North and South Atlantic SSTA on the zonal/meridional wind (U/V) at 300hPa in P1, which disappeared

in P2, as shown in Fig. 7. This was consistent with the variation of Atlantic SSTA's contribution to

DUCMASS–Niño-3 relationship, i.e., during P1, the Atlantic SSTA pattern was featured with a Niña type

(Fig. 3 (a)), thus the South Atlantic presented stronger influence on the atmospheric circulation over

South Asia, which weakened the impact of ENSO on DUCMASS; while in P2, the negative North

Atlantic SSTA (Fig. 3 (b)) decreased the SSTA gradient between North and South Atlantic and offset the

effect of the Niña pattern, which weakened the response of atmospheric circulation on North and South

Atlantic SSTA gradient and strengthened the DUCMASS–Niño-3 relationship.
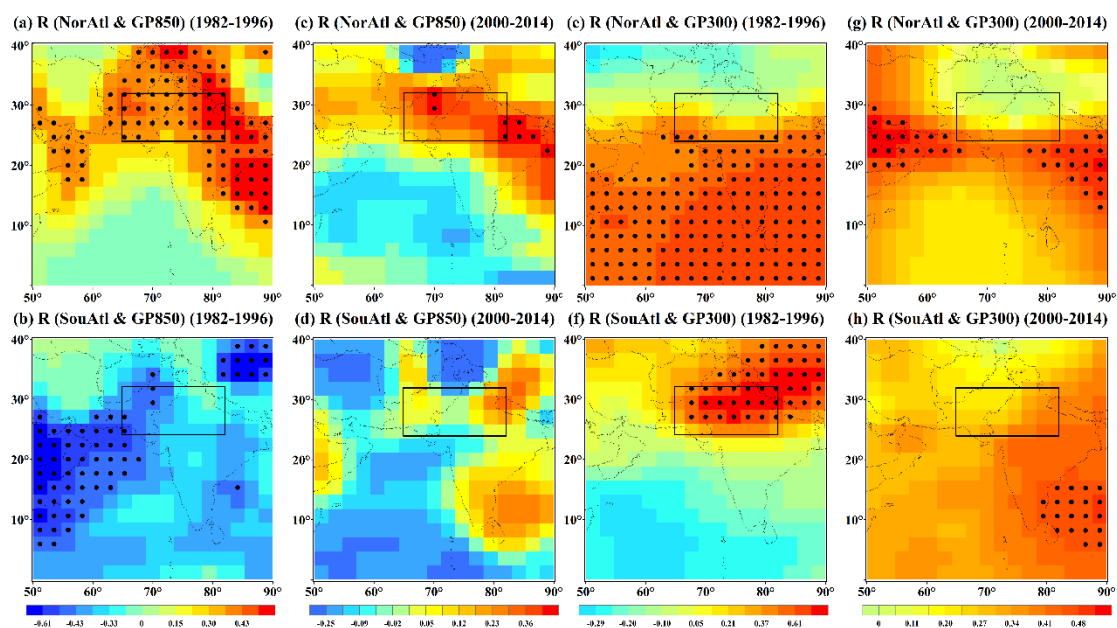
Figure 6: Correlation between spring (Mar.–May) tropical North and South Atlantic SSTA (NorAtl/SouAtl) with ENSO signal removed and geopotential height (GP) at 850hPa (a)–(d) as well as 300hPa (e)–(h) in dust season (Jun.–Jul.). (Correlations that passed the 90% confidence level were marked by black dots).

Figure 7: Correlation between spring (Mar.–May) tropical North and South Atlantic SSTA (NorAtl/SouAtl) with ENSO signal removed and zonal wind (U) (a)–(d) as well as meridional wind (V) (e)–(h) at 300hPa in dust season (Jun.–Jul.). (Correlations that passed the 90% confidence level were marked by black dots).

In order to verify the inhibitory effect of Atlantic SSTA pattern on the DUCMASS–Niño-3 relationship, we analyzed the regression of ASGI onto the local conditions that directly influenced DUCMASS, such as precipitation (PPT), soil moisture (SoilM), Normalized Difference Vegetation Index (NDVI), and air flow. Figure 8 showed that the regression coefficients between ASGI and SoilM as well as PPT and NDVI (not shown) were opposite to that between Niño-3 and SoilM during P1, while during P2, the abovementioned differences were weakened. Besides, Figure 9 demonstrated that the regression coefficients between Niño-3 and velocity potential (VP) as well as wind field at 200hpa and 850hPa were also contrary to the regression coefficients between ASGI and those factors, indicating the opposite effect of ASGI and ENSO on local wind field and convection. All of those proved the inhibitory effect of Atlantic SSTA pattern on the DUCMASS–Niño-3 relationship during P1.

294
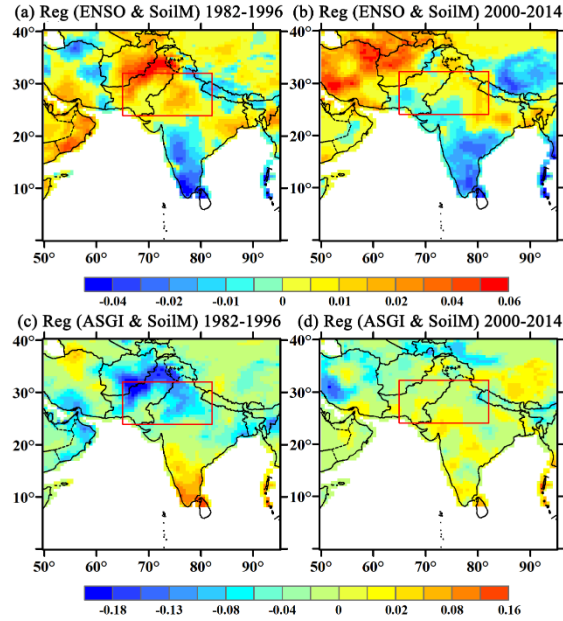
Figure 8: (a)–(b) Regression of ENSO with ASGI-related signals removed onto SoilM in dust season (Jun.–Jul.); (c)–(d) Regression of ASGI with ENSO-related signals removed onto SoilM in dust season (Jun.–Jul.).

297
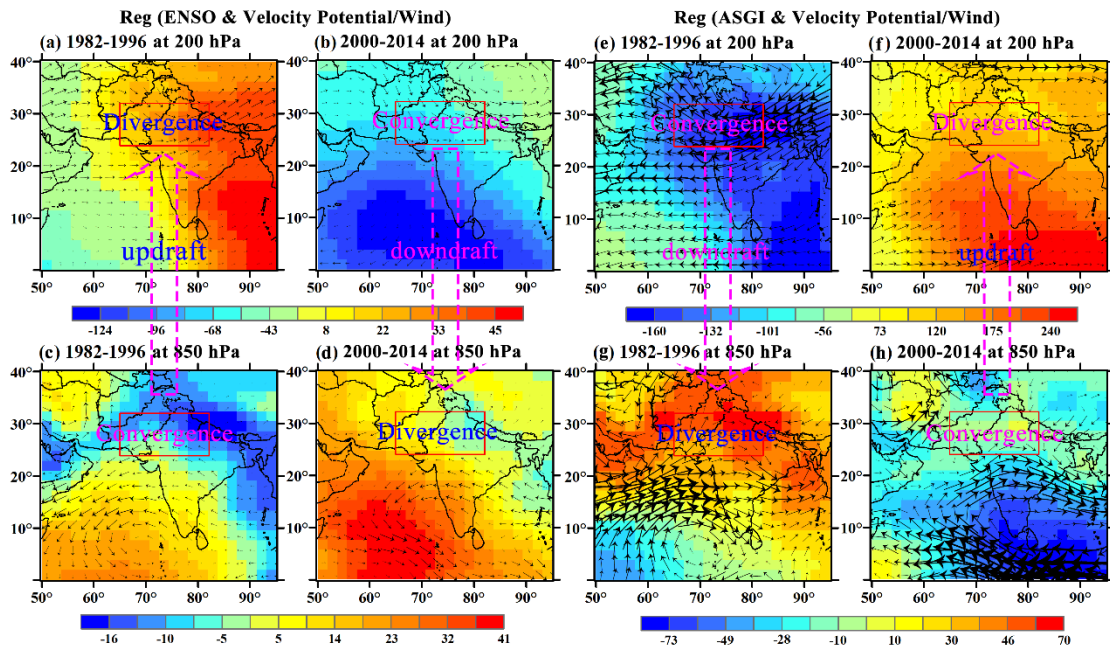
Figure 9: (a)–(d) Regression of ENSO with ASGI-related signals removed onto velocity potential (VP) and wind at 200hPa and 850hPa in dust season (Jun.–Jul.); (e)–(h) Regression of ASGI with ENSO-related signals removed onto velocity potential and wind at 200hPa and 850hPa in dust season (Jun.–Jul.).

3.2.2 Tropical Indian ocean SSTA pattern

This study explored the effect of Indian ocean SSTA pattern on the DUCMASS–Niño-3 relationship. The covariability between the western Pacific and Indian Ocean has been widely recognized by previous studies (Kug et al., 2005; Wang et al., 2003; Watanabe and Jin, 2002). ENSO can affect the Indian Ocean

305   SST in the form of Walker circulation and the Indian Ocean variability can also modulate the ENSO

306   variability (Kug et al., 2005; Wu and Kirtman, 2004; Yu et al., 2002). It is known that ENSO mainly

307   influences the monsoon rainfall of South Asia through changing the SST of Indian ocean (Krishnamurthy

308   and Kirtman, 2003; Srivastava et al., 2019). Du et al. (2009) indicated that the North Indian Ocean

309   warming displayed two peaks in Nov.–Dec.(-1) and Jun.–Aug.(0), with the second peak larger in

310   magnitude. Cherchi and Navarra (2013) also pointed out that the connection between ISM and Indian

311   ocean SST pattern was mostly confined in summer and autumn. Besides, compared to Atlantic, the Indian

312   ocean is closer to the South Asian dust source, thus it takes less time to transmit the signal (partially

313   through wave train propagation) from the Indian ocean to the dust source than that from the Atlantic.

314   Given all of that, the Indian ocean SST used in this study was the summer average that was concurrent

315   with the dust season (Jun.–Jul.).

316   The relationship between DUCMASS and Niño-3 with Indian ocean SST signal removed also

317   experienced decadal variation. Figure 10 (a) showed that the correlation between Niño-3 and DUCMASS

318   was obviously reduced when the tropical western Indian ocean SSTA (TWISST) was removed from

319   Niño-3. As illustrated by Fig. 10 (b), during P1, TWISST weakened this correlation while no significant

320   contribution was observed during P2. Thus, it is hypothesized that TWISST weakened the impact of

321   ENSO on DUCMASS during P1. However, when the IOD (rather than TWISST) was considered, the

322   correlation between Niño-3 and DUCMASS kept the same when IOD was removed from Niño-3,

323   indicating that IOD exhibited no significant impact on the correlation between Niño-3 and DUCMASS.

324   Clark et al. (2000) showed that the SST in the central Indian Ocean exhibited stronger correlation with

325   the Indian precipitation than that in the Arabian Sea and northwest of Australia. Cherchi and Navarra

326   (2013) also pointed out that when the eastern and western poles of the IOD were considered separately,

327   the western side exhibited the largest correlation. Thus, the TWISST was considered when exploring the

328   effect of Indian ocean SSTA pattern on the DUCMASS–Niño-3 relationship.
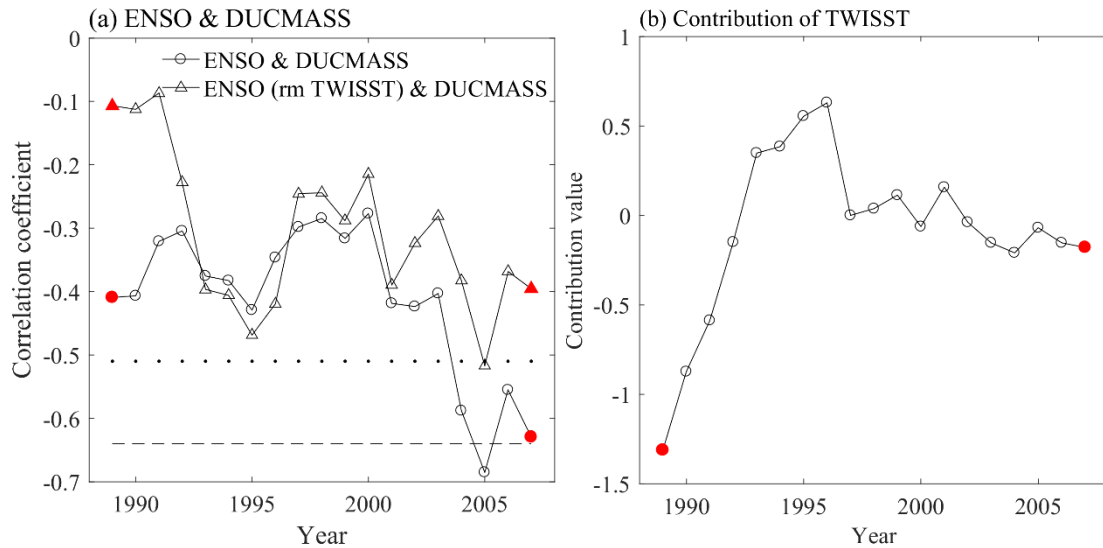
Figure 10: (a) The 15-year sliding correlation between DUCMASS and Niño-3 with and without TWISST-related signals removed; (b) Sliding contribution of TWISST to DUCMASS–Niño-3 relationship. The two red filled markers represented the 15-year window spanning from 1982 to 1996 and 2000 to 2014, respectively. The x-axis denotes the middle year of the period under analysis.

The spatial coupling mode between DUCMASS and tropical Indian ocean SSTA showed that the cold tropical western Indian ocean and warm tropical eastern Indian ocean were coupled with higher DUCMASS over the northern and northwestern India. This pattern was not impacted by ENSO since the MCA results with ENSO-related signals removed were similar with that including the ENSO-related signals, as shown in Fig. 11. Figures 12–14 further illustrated the influence mechanism of Indian ocaean SSTA pattern onto DUCMASS. Figure 12 showed that during P1, the regression coefficients between ENSO and PPT were opposite to the that between TWISST and PPT, while during P2, the regression coefficient between ENSO and DUCMASS as well as that between TWISST and DUCMASS were all positive. The similar changes were also seen when the effects of ENSO/TWISST on SoilM (Fig. 13), VP and wind field (Fig. 14) were considered. These illustrated the opposite effect of TWISST and ENSO on the key factors that influence the dust concentration, i.e., the local wind field and surface conditions. The above results further verified the inhibitory effect of Indian ocean SST pattern on the DUCMASS–Niño-3 relationship during P1, as well as the promotional effect during P2.
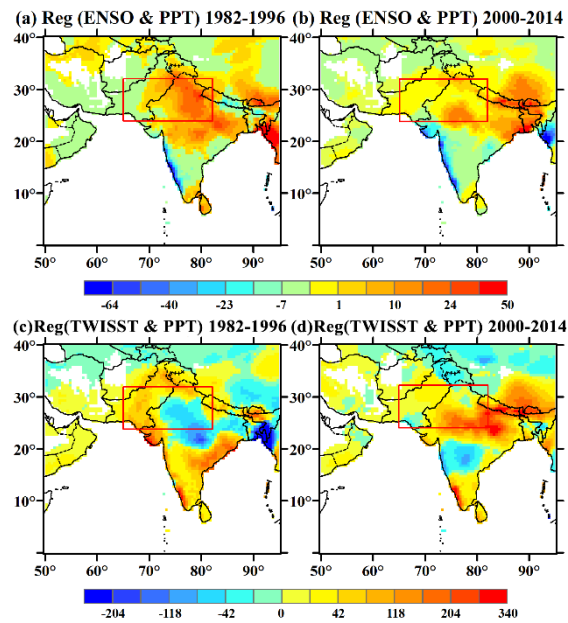
347
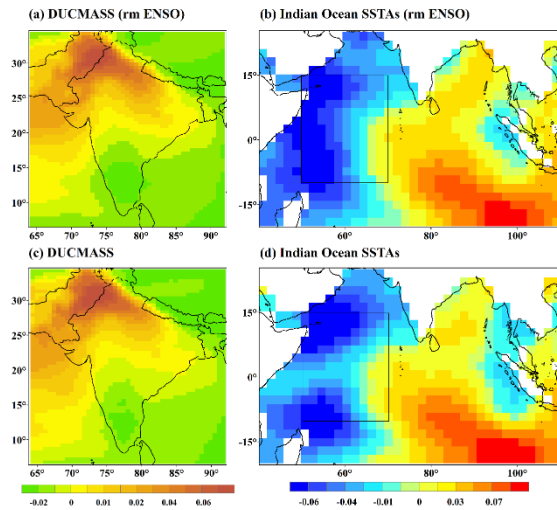
Figure 11: Spatial correlation between summer (Jun.-Jul.) tropical Indian ocean SSTA (TWISSTA) and DUCMASS of the first mode of the MCA analysis in 1982–2014. The first MCA mode of (a) the DUCMASS, and (b) the summer (Jun.-Jul.) tropical Indian ocean SSTA with ENSO-related signals removed. (c)–(d) As in (a)–(b), but for the original series including the ENSO signal.
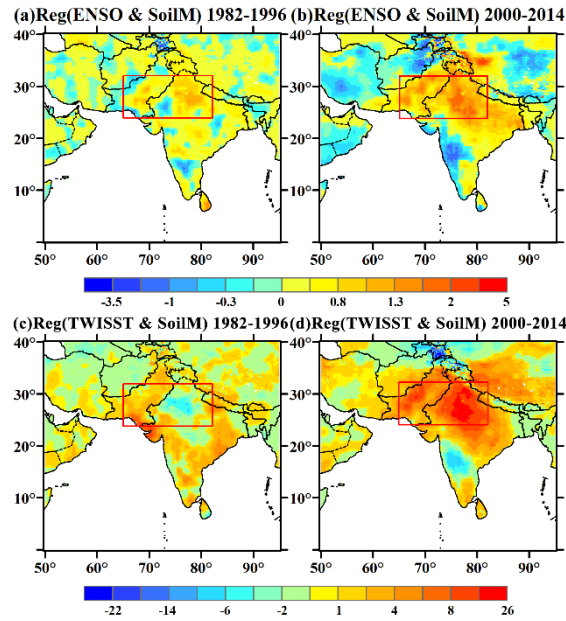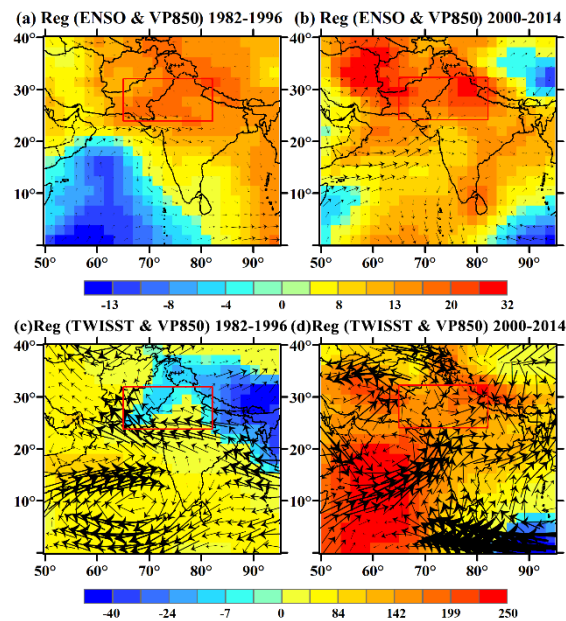
352

Figure 12: (a)–(b) Regression of ENSO with TWISST-related signals removed onto PPT in dust season (Jun.–Jul.); (c)–(d) Regression of TWISST with ENSO-related signals removed onto PPT in dust season (Jun.–Jul.).

17

(a)Reg(ENSO & SoilM) 1982-1996 (b)Reg(ENSO & SoilM) 2000-2014

(c)Reg(TWISST & SoilM) 1982-1996(d)Reg(TWISST & SoilM) 2000-2014

355

356 **Figure 13: (a)–(b) Regression of ENSO with TWISST-related signals removed onto SoilM in dust season**

357 **(Jun.–Jul.); (c)–(d) Regression of TWISST with ENSO-related signals removed onto SoilM in dust season**

358 **(Jun.–Jul.).**

(a) Reg (ENSO & VP850) 1982-1996 (b) Reg (ENSO & VP850) 2000-2014

(c)Reg (TWISST & VP850) 1982-1996 (d)Reg (TWISST & VP850) 2000-2014

359

360 **Figure 14: (a)–(b) Regression of ENSO with TWISST-related signals removed onto velocity potential at**

361 **850hPa (VP850) and wind in dust season (Jun.–Jul.); (c)–(d) Regression of TWISST with ENSO-related**

362 **signals removed onto velocity potential at 850hPa (VP850) and wind in dust season (Jun.–Jul.).**

363 **3.2.3 Pacific Decadal Oscillation**

364   It is suggested that the PDO can influence the interannual variability of ISMR by enhancing the

365 ENSO–ISMR relationship when ENSO and PDO were in-phase, while weakening the relationship when

18

366 they were out of phase (Dong et al., 2018; Krishnamurthy and Krishnamurthy, 2014). However, it is

367 unclear whether PDO is responsible for the shift of the DUCMASS–Niño-3 relationship. Table 2 listed

368 the years with different phases of ENSO and PDO as well as years when ENSO and PDO are in (out of)

369 phase separately. The correlation coefficient between ENSO and DUCMASS and significance level were

370 also given. It demonstrated that the PDO significantly strengthened the correlation between ENSO and

371 DUCMASS as the coefficient turned from –0.39 (P>0.1) when PDO and ENSO were out of phase to –

372 0.69 (P<0.01) when they were in phase.

373 **Table 2: List of individual and combined wintertime ENSO–PDO years during 1982–2014.**

| Events	Phase	
	Positive	Negative
ENSO	1983, 1987, 1988, 1991, 1993–1995, 1998, 2003, 2005, 2007, 2010, 2015, 2016, 2019	1982, 1984–1986, 1989, 1996, 1997, 1999–2001, 2006, 2008, 2009, 2011, 2012, 2014
PDO	1981–1988, 1996–1998, 2001, 2003–2006, 2010, 2014–2019	1989, 1991, 1995, 1999, 2000, 2002, 2008, 2009, 2011, 2012
ENSO×PDO	1983, 1987–1989, 1998–2000, 2003, 2005, 2008–2012	1982, 1984–1986, 1991, 1995–1997, 2001, 2006, 2014
R (Niño-3 & DUCMASS)	–0.69 (P<0.01)	–0.39 (P>0.1)

374   Table 2 revealed that P2 includes most of years (8 out of 14) when ENSO and PDO were in-phase,

375 i.e., 2000, 2003, 2005, and 2008–2012, while most of the out-of-phase years (8 out of 11) appeared in

376 P1, i.e., 1982, 1984–1986, 1991, 1995, 1996, and 1997. Simultaneously, the winter Niño-3 exhibited

377 lower correlation with DUCMASS in P1 when most of ENSO years were accompanied with anti-phase

378 PDO. In addition, the quantitative contribution of PDO shown in Fig. 15 further confirmed that the PDO

379 strengthened the impact of ENSO on DUCMASS in P2 while the contribution was close to 0.0 in P1. All

380 those demonstrated that the phase shift of PDO plays an important role in modulating the revolution of

381 DUCMASS–Niño-3 relationship.
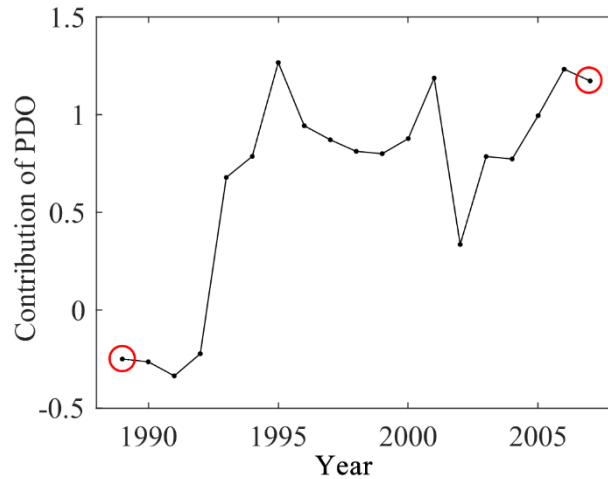
Figure 15: Sliding contribution of PDO to DUCMASS–Niño-3 relationship. The two circles represented the 15-year window spanning from 1982 to 1996 and 2000 to 2014, respectively.

Figure 16 revealed the influence mechanism of PDO onto DUCMASS. During P1, the 200hPa velocity potential in the positive PDO years exhibited a decrease (convergence) over the eastern tropical Pacific and an increase (divergence) over the tropical Indian Ocean and Indian subcontinent (Fig. 16 (a)). The upper-level divergence over India and the adjacent seas corresponded to the anomalous ascending motion, which promoted ISMR and consequently suppressed the dust storms over South Asia. Meanwhile, an anomalous cyclone developed to the north of India due to the enhanced convection. The westerlies on the southern flank of the cyclonic anomaly transported wet air from the Arabian Sea to the northwest of India (Huang et al., 2020), which further inhibited dust emissions. While in the negative PDO years during P2, the 200hPa velocity potential exhibited a decrease (convergence) over India, corresponding to an anomalous descending motion, as shown in Fig. 16 (b). This descending flow suppressed the Indian monsoon convection and rainfall, which consequently enhanced dust emissions. Similarly, an anomalous cyclone developed over the south of India. The easterlies on the northern flank of the cyclonic anomaly advected relatively drier air from the Eurasian continent to the northern India (Parker et al., 2016), which favored dust emissions. The difference of flow movements and their effects on dust activities between positive and negative PDO years was consistent with that between El Niño and La Niña years, which further proved that PDO could significantly strengthen the effect of ENSO on DUCMASS when it was in phase with ENSO.

(a) Reg of VP & UV at 200hPa onto PDO in 1982-1996
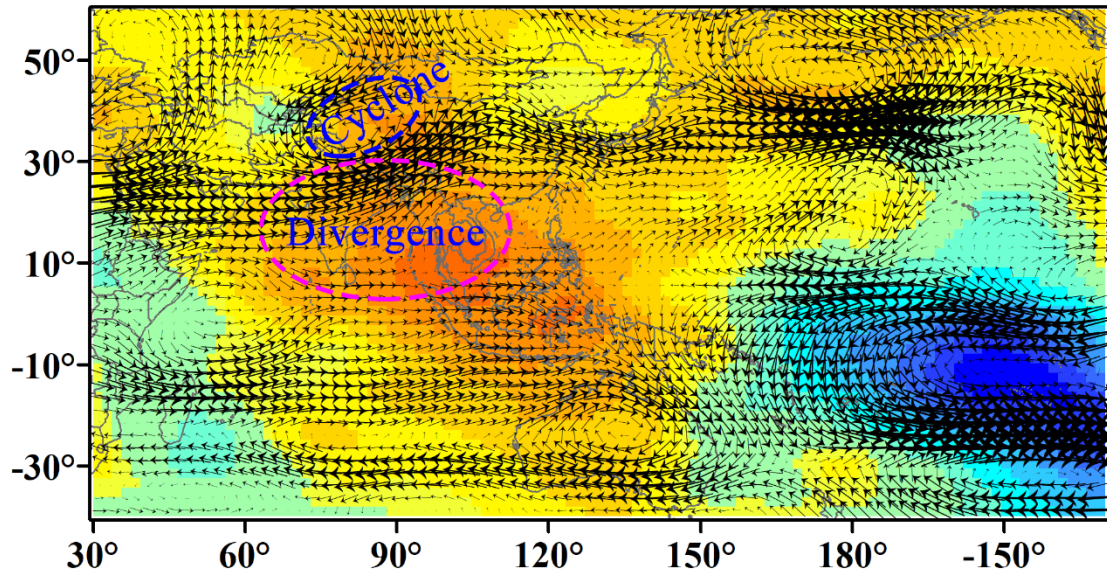
(b) Reg of VP & UV at 200hPa onto PDO in 2000-2014
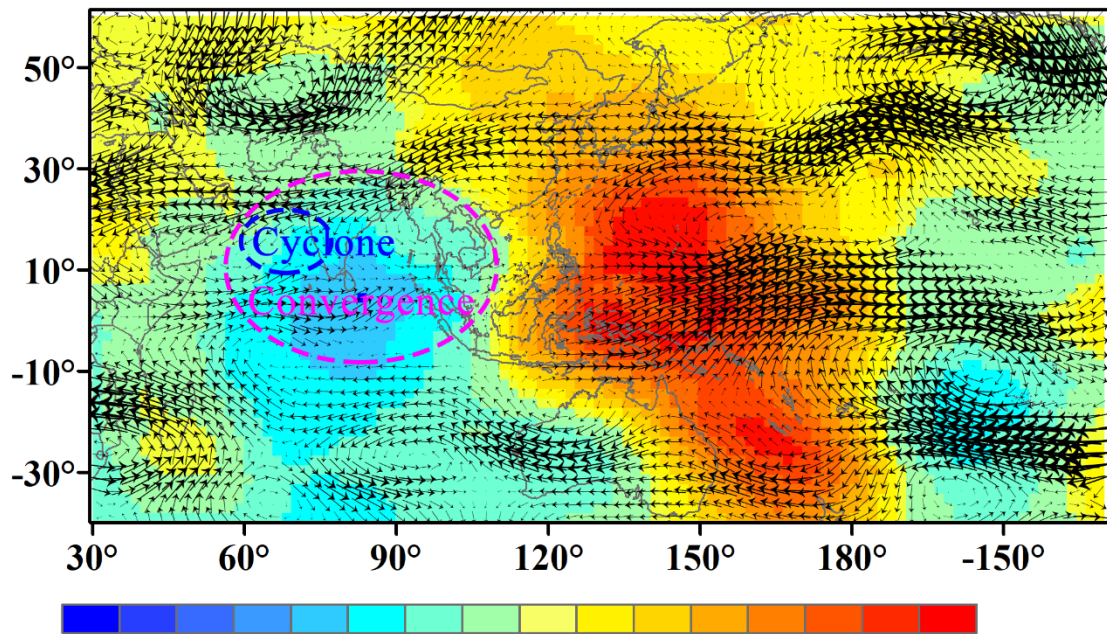
Figure 16: (a) Regression of summer (Jun.-Jul.) velocity potential at 200hPa onto previous winter PDO (averaged from Nov. to Jan.) overlaid with the average of summer wind in positive PDO years during 1982–1996; (b) Regression of summer velocity potential at 200hPa onto previous winter PDO overlaid with the average of summer wind in negative PDO years during 2000–2014.

4 Discussion

4.1 Response of Atlantic SSTA pattern to CT/EM ENSO

It was reported that the interdecadal shift of tropical Atlantic SSTA pattern was a response to the

410 multi-year ENSO events (Tokinaga et al., 2019). The multi-year ENSO event, namely continuing ENSO

411 (CT ENSO), was a situation where the summer ENSO SSTA continued from the preceding year. Another

412 type of ENSO, which was called as emerging ENSO (EM ENSO), was characterized as late Atlantic

413 SSTA response that started from June. The CT ENSO primarily dominated during P1, while P2 was

414 dominated by EM ENSO (Yang and Huang, 2021). The impact of the two types of ENSO on the shift of

415 the DUCMASS–Niño-3 relationship were examined. Table 3 showed that ASGI was significantly

416 correlated with Niño-3 in the CT ENSO years, which was not observed in the EM ENSO years.

417 Simultaneously, DUCMASS was significantly related to Niño-3 only in the EM ENSO years. The

418 composite correlation difference between CT and EM ENSOs was consistent with that between the

419 period of P1 and P2, indicating that the shift of Atlantic SSTA pattern, which was prominently modulated

420 by the type of ENSO, plays an important role in modulating the DUCMASS–Niño-3 relationship.

421 **Table 3: Correlation between ASGI and Niño-3 as well as DUCMASS in two different phases (* and ***
422 indicate the correlations that are significant on a 0.1 and 0.01 level, respectively).**

| R	CT ENSO	EM ENSO	P1	P2
ASGI & Niño-3	0.78 (***)	0.19	0.73 (***)	0.46 (*)
DUCMASS & Niño-3	-0.60 (*)	-0.75 (***)	-0.51 (*)	-0.67 (***)

423

424 **4.2 Response of Indian ocean SSTA pattern to CT/EM ENSO**

425 As discussed in Sect. 3.2.2, ENSO can affect the Indian Ocean SST and the Indian Ocean variability

426 can also modulate the ENSO variability (Kug et al., 2005; Wu and Kirtman, 2004; Yu et al., 2002). It is

427 known that during CT ENSO years, the ENSO event in summer primarily starts from the preceding

428 winter, while in EM ENSO years, the ENSO event mainly emerges in late spring (Yang and Huang, 2021).

429 Correspondingly, the associated Indian Ocean SST oscillation also varies in these two different ENSO

430 years. In order to explore whether the different types of ENSO impacted the DUCMASS over the

431 northwestern South Asia through adjusting the duration of the temperature anomaly, we compared the

432 SST and the variance of the monthly SSTA from (–1) Sep. to (0) May over the tropical western Indian

433 ocean (TWISSTA).

434 Figure 17 (a) showed that the variances in the EM La Niña years were generally larger than that in

22

435 the CT La Niña years, while the variances in the EM El Niño years were generally smaller than that in

436 the CT El Niño years. Concurrently, the difference of DUCMASS in El Niño and La Niña years was

437 obvious in the EM ENSO period with higher values appeared in La Niña years (Fig. 17 (b)). However,

438 in the CT ENSO period, no significant difference was observed between El Niño and La Niña years.

439 Therefore, it is hypothesized that the EM ENSO conditions, which was associated with higher TWISST

440 variance, were more favorable to trigger the variation of DUCMASS. Yang and Huang (2021) reported

441 that P1 was primarily dominated by CT ENSOs while EM ENSOs primarily controlled during P2.

442 Combined with abovementioned hypothesis, the correlation between DUCMASS and Niño-3 should be

443 higher in P2, which was consistent with the interdecadal change of this relationship. Figure 17 (c) further

444 revealed the influence mechanism of TWISSTA onto DUCMASS. It showed that compared to CT ENSO

445 type, the difference of PPT between El Niño and La Niña years was more significant in the EM ENSO

446 years, in addition, the PPT in La Niña years (with high TWISSTA variance) was lower than that in El

447 Niño years (with low TWISSTA variance), which was contrary to the difference of DUCMASS between

448 those two types of ENSO years. While when other atmospheric factors were considered, such as land

449 cover and winds at multi-layers, no similar change was observed. This indicated that the Indian Ocean

450 SSTA, which was also remarkably modulated by the type of ENSO, impacted DUCMASS by adjusting

451 the PPT and further influenced the relationship between ENSO and DUCMASS.
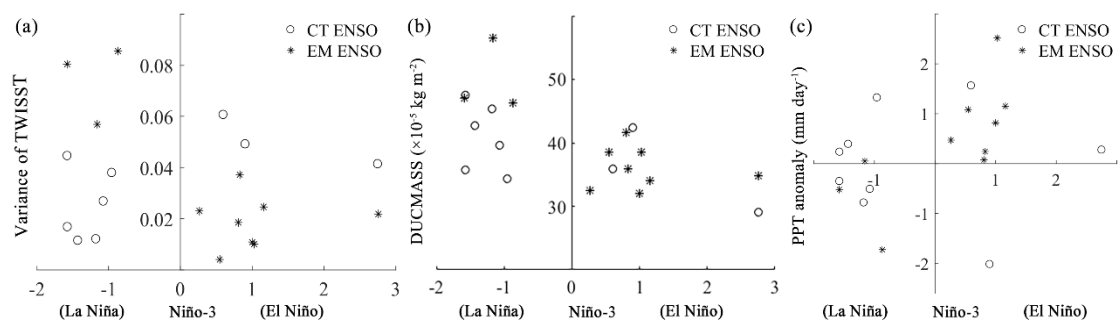
452

453 **Figure 17: Scatter diagram between (a) variance of the monthly TWISSTA from (–1) Sep. to (0) May, (b)**

454 **DUCMASS, and (c) PPT anomaly and Niño-3 index separately for continuing (CT) and emerging (EM) ENSO.**

455 **4.3 Uncertainty in analyzing the contribution of the influence factors**

456   The contributions of those abovementioned factors to the interdecadal shift of ENSO-DUCMASS

457 relationship were analyzed based on the linear regression model. However, the linear regression model

458 would definitely bring uncertainty to the results (Guo et al., 2017) and may not be sufficient to verify the

459　cause and effect. Thus, the numerical models are suggested for future research to quantify the

460　contribution of those factors to the shift of ENSO–DUCMASS relationship. However, before such

461　quantitative study the regression analysis is indispensable to identify the possible driving factors. In this

462　context, it is undeniable that this study provides new sights to the dust storm-related numerical simulation

463　by taking account of the teleconnections and their influence mechanisms.

464　　　In addition, while analyzing the effects of different types of ENSO event, we compared the variance

465　of TWISST and DUCMASS under the two types of ENSO periods, as shown in Fig. 17. It showed that

466　only eight EM ENSO years were identified and the number of PDO years that were in or out of phase

467　with ENSO were also insufficient. The statistical results acquired from the insufficient number of

468　samples could also be explained by the random events (Pallikari, 2004). In order to verify this conclusion,

469　we calculated the interannual correlation between the variance of TWISST and DUCMASS from 1982

470　to 2014. Even so, the significant interannual correlation does not guarantee the significant link between

471　different types of ENSO. Therefore, longer time series with valid samples (i.e., CT/EM ENSO and PDO

472　years) are needed to further validate the influence of ENSO types on the ENSO–DUCMASS relationship

473　in the future. Alternatively, using numerical model to simulate the teleconnection pattern of ENSO over

474　South Asia under different types of ENSO is also favorable.

475　　　Except for the large-scale atmospheric circulation, the anthropogenic land-use management could

476　also play an important role in the interdecadal variability of ENSO–DUCMASS relationship (Kumar et

477　al., 1999), which should be considered in the future researches.

478　　　The dust activities analyzed in this study were from the dust season, i.e., Jun.–Jul., which were part

479　of monsoon season (Jun.–Sep.) (Babu et al., 2013), however, the dust activities during pre-monsoon

480　season (Mar.–May or Apr.–May) were also a hot topic (Babu et al., 2013; Lakshmi et al., 2017, 2019).

481　Therefore, we analyzed the interdecadal change of the ENSO impact on DUCMASS during dust season

482　(Jun.–Jul.) and pre-monsoon (Mar.–May or Apr.–May) separately, to find that the significant interdecadal

483　change occurred only when the DUCMASS during dust season was considered. As for that during pre-

484　monsoon season, there should be some other factors that influenced its interdecadal change, which will

485　be discussed in the future study.

486　**4.4 Precision validation of MERRA-2 dust concentration dataset**

487   It is known that the nonspherical aerosol optical depth retrieved from satellite, concentration of

488   PM2.5/PM10 and coarse mode aerosol optical depth acquired from observation stations represent

489   extinction characteristics of dust aerosols in the whole atmospheric column, thus they can be used to

490   validate the dust column concentration datasets but not appropriate for the validation of dust emission,

491   which reflect the dust loading lifted from ground. The dust dataset used in this study was the dust column

492   concentration "Dust Column Mass Density-PM$_{2.5}$", thus the PM$_{2.5}$, coarse mode aerosol optical depth

493   acquired from AERONET (AERONET/DOD), and nonspherical aerosol optical depth retrieved from

494   MISR (MISR/DOD) was utilized to validate the precision of DUCMASS dataset. The time coverage and

495   continuity of satellite and observation-based products lagged behind the MERRA-2 datasets, thus only

496   several stations over the dust belt with relatively longer time series were chosen. They were Kanpur (26.5°

497   N, 80.2° E. Time span: 2001–2021), Sede Boker (30.9° N, 34.8° E. Time span: 2007–2019), and

498   Tamanrasset INM (22.8° N, 5.5° E. Time span: 2007–2019). The MISR/DOD, PM2.5, and dust variables

499   from MERRA-2 were the regional average within 1° of the corresponding station. No dust emission was

500   observed over the Kanpur and Tamanrasset INM station. Besides, the datasets over the study area

501   (represented by Thar desert in Fig. 18 (a)) were also accounted and the AERONET/DOD was obtained

502   from the nearest Kanpur station. For the study area, PM$_{2.5}$ was chosen as the reference dataset (A) because

503   the study area was not overlapped with the Kanpur station, while AERONET/DOD was chosen as the

504   reference data for other stations.
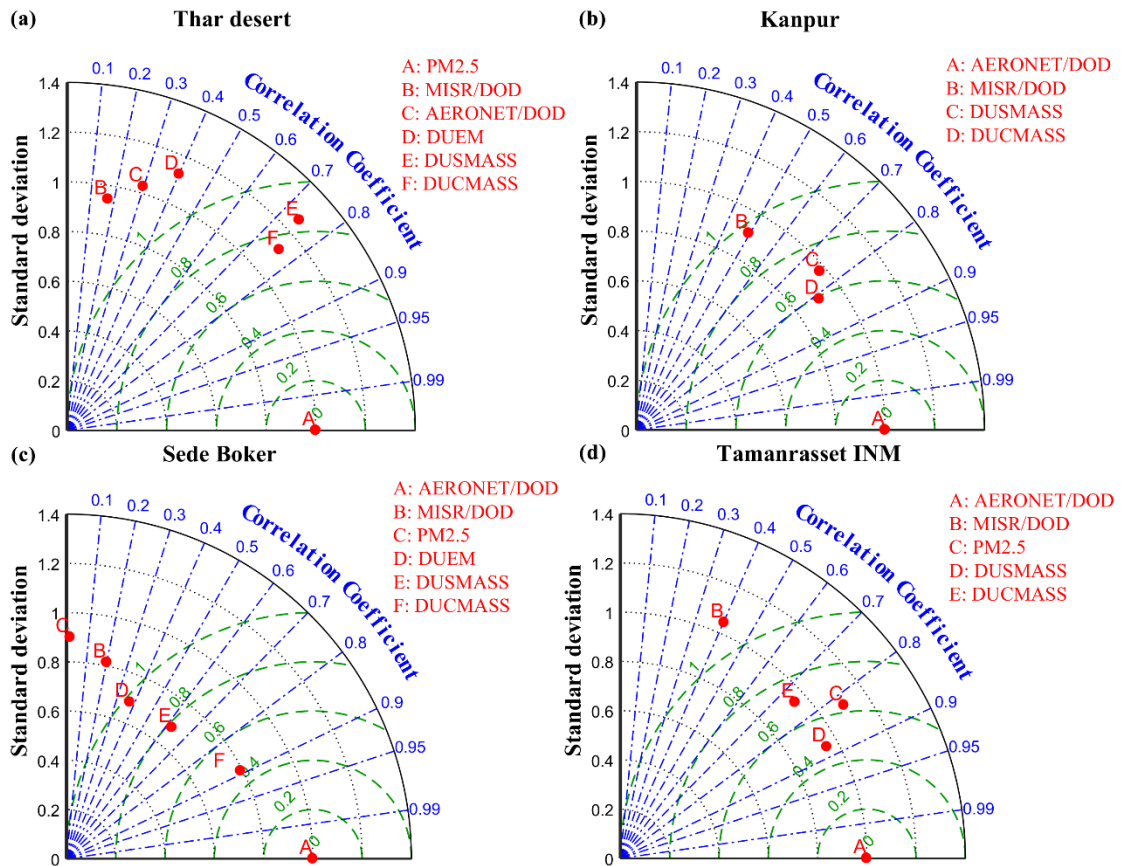
Figure 18: Precision validation of MERRA-2 dust concentration datasets

Figure 18 (a) compared the precision of MISR/DOD, AERONET/DOD, dust emission (DUEM), surface dust mass concentration (DUSMASS), and DUCMASS with that of $PM_{2.5}$, it showed that no significant correlation was observed between AERONET/DOD and $PM_{2.5}$ because this study area did not coincide with the Kanpur station. However, the correlations between $PM_{2.5}$ and DUSMASS as well as DUCMASS were significant ($R>0.7$, RMSE<0.9) and stronger than that between $PM_{2.5}$ and DUEM. Figure 18 (b) showed the precision of MISR/DOD, DUSMASS, and DUCMASS compared with AERONET/DOD over the Kanpur station. The results indicated that both DUSMASS and DUCMASS were significantly correlated with AERONET/DOD ($R>0.7$, RMSE<0.8). In addition, the comparison results over the other two stations also indicated that DUSMASS and DUCMASS were significantly correlated with AERONET/DOD, while the relationship between DUEM and AERONET/DOD was weak, as shown in Figs. 18 (c)–(d). The above results demonstrated that the DUCMASS from MERRA-2 was strongly consistent with MISR/DOD, AERONET/DOD, and $PM_{2.5}$, indicating that the DUCMASS datasets used in this study were with high precision.

5 Conclusions

In the study, we revealed the interdecadal change of the ENSO impact on DUCMASS over the northwestern South Asia from 1982 to 2014, and further investigated the factors contributing to the shifts of the responses of DUCMASS to the wintertime ENSO. It was found that the ENSO–DUCMASS relationship shifted from weak negative relation during 1982–1996 to significant negative correlation during 2000–2014. The change of Atlantic and Indian ocean SSTA pattern weakened the impact of wintertime ENSO on dust activities over the northwestern South Asia during 1982–1996, while PDO tended to strengthen ENSO's effect on dust activities when it was in phase with ENSO. Both the Atlantic and Indian Ocean SSTA patterns were modulated by the duration of ENSO events (i.e., continuing and emerging ENSO). The current results are based solely on the linear regression, and further studies integrating numerical models and longer time series are needed to validate the results. Nevertheless, this study indeed found multiple large-scale factors that could impact the interdecadal interaction between ENSO and dust activities over the northwestern South Asia. Given that it is possible to forecast the change of some large-scale atmospheric circulation patterns, the results of this study could provide new insight to the prediction of dust storm trend in the near future based on the variability of ENSO–DUCMASS relationship.

Data availability

The data can be downloaded for free from the corresponding website which were listed in the text.

Author contribution

L.S. designed the study, performed the analysis with feedback from J.Z. and F.Y., and wrote the paper that was reviewed by J.Z., F.Y., D.Z., J.W., X.M., and Y.L.. All the authors discussed the results.

Competing interests

The authors declare that they have no conflict of interest.

Acknowledgments

References

Abish, B. and Mohanakumar, K.: Absorbing aerosol variability over the Indian subcontinent and its increasing dependence on ENSO, Glob. Planet. Change, 106, 13–19, doi:10.1016/j.gloplacha.2013.02.007, 2013.

Ashok, K., Behera, S. K., Rao, S. A., Weng, H. and Yamagata, T.: El Nino Modoki and its possible teleconnection, J. Geophys. Res., 112, C11007, 2007.

Augustyn, A., Zeidan, A., Zelazko, A., Eldridge, A., McKenna, A., Tikkanen, A., Gadzikowski, A., Schreiber, B. A., Duignan, B., Mahajan, D., Promeet, D., Goldstein, E. and Rodriguez, E.: Thar Desert, Encycl. Br. [online] Available from: https://www.britannica.com/place/Thar-Desert, 2019.

Avila, A.: The chemical composition of dust transported in red rains—its contribution to the biogeochemical cycle of a holm oak forest in Catalonia (Spain), Atmos. Environ., 32(2), 179–191, 1998.

Babu, S. S., Manoj, M. R., Moorthy, K. K., Gogoi, M. M., Nair, V. S., Kompalli, S. K., Satheesh, S. K., Niranjan, K., Ramagopal, K., Bhuyan, P. K. and Singh, D.: Trends in aerosol optical depth over Indian region: Potential causes and impact indicators, J. Geophys. Res. Atmos., 118(20), 11,794-11,806, doi:10.1002/2013JD020507, 2013.

Banerjee, P. and Kumar, S. P.: ENSO modulation of interannual variability of dust aerosols over the northwest Indian Ocean, J. Clim., 29(4), 1391–1415, doi:10.1175/JCLI-D-15-0039.1, 2016.

571   Banerjee, P., Satheesh, S. K., Moorthy, K. K., Nanjundiah, R. S. and Nair, V. S.: Long-range transport

572   of mineral dust to the northeast Indian Ocean: Regional versus remote sources and the implications,

573   J. Clim., 32(5), 1525–1549, doi:10.1175/JCLI-D-18-0403.1, 2019.

574   Behrooz, R. D., Esmaili-Sari, A., Bahramifar, N. and Kaskaoutis, D. G.: Analysis of the TSP, PM10

575   concentrations and water-soluble ionic species in airborne samples over Sistan, Iran during the

576   summer dusty period, Atmos. Pollut. Res., 8(3), 403–417, 2017.

577   Bollasina, M. A., Ming, Y. and Ramaswamy, V.: Anthropogenic aerosols and the weakening of the south

578   asian summer monsoon, Science (80-.)., 334(6055), 502–505, doi:10.1126/science.1204994, 2011.

579   Bozlaker, A., Prospero, J. M., Fraser, M. P. and Chellam, S.: Quantifying the contribution of long-range

580   saharan dust transport on particulate matter concentrations in Houston, Texas, using detailed

581   elemental analysis, Environ. Sci. Technol., 47(18), 10179–10187, doi:10.1021/es4015663, 2013.

582   Buchard, V., Randles, C. A., da Silva, A. M., Darmenov, A., Colarco, P. R., Govindaraju, R., Ferrare,

583   R., Hair, J., Beyersdorf, A. J., Ziemba, L. D. and Yu, H.: The MERRA-2 aerosol reanalysis, 1980

584   onward. Part II: Evaluation and case studies, J. Clim., 30(17), 6851–6872, doi:10.1175/JCLI-D-16-

585   0613.1, 2017.

586   Cai, W., Borlace, S., Lengaigne, M., Van Rensch, P., Collins, M., Vecchi, G., Timmermann, A., Santoso,

587   A., Mcphaden, M. J., Wu, L., England, M. H., Wang, G., Guilyardi, E. and Jin, F. F.: Increasing

588   frequency of extreme El Niño events due to greenhouse warming, Nat. Clim. Chang., 4(2), 111–116,

589   doi:10.1038/nclimate2100, 2014.

590   Chauhan, S. S.: Desertification control and management of land degradation in the Thar desert of India,

591   Environmentalist, 23(3), 219–227, doi:10.1023/B:ENVR.0000017366.67642.79, 2003.

592   Chen, Y.-S., Sheen, P.-C., Chen, E.-R., Liu, Y.-K., Wu, T.-N. and Yang, C.-Y.: Effects of Asian dust

593   storm events on daily mortality in Taipei, Taiwan., Environ. Res., 95(2), 151–155,

594   doi:10.1016/j.envres.2003.08.008, 2004.

595   Cherchi, A. and Navarra, A.: Influence of ENSO and of the Indian Ocean Dipole on the Indian summer

596   monsoon variability, Clim. Dyn., 41(1), 81–103, doi:10.1007/s00382-012-1602-y, 2013.

597   Clark, C. O., Cole, J. E. and Webster, P. J.: Indian Ocean SST and Indian summer rainfall: Predictive

598   relationships and their decadal variability, J. Clim., 13(14), 2503–2519, doi:10.1175/1520-

599   0442(2000)013<2503:IOSAIS>2.0.CO;2, 2000.

600   Dong, B., Dai, A., Vuille, M. and Timm, O. E.: Asymmetric modulation of ENSO teleconnections by

601   the interdecadal Pacific oscillation, J. Clim., 31(18), 7337–7361, doi:10.1175/JCLI-D-17-0663.1,

602   2018.

603   Du, Y., Xie, S. P., Huang, G. and Hu, K.: Role of air-sea interaction in the long persistence of El Niño-

604   induced north Indian Ocean warming, J. Clim., 22(8), 2023–2038, doi:10.1175/2008JCLI2590.1,

605   2009.

606   Easterling, D. R. and Wehner, M. F.: Is the climate warming or cooling?, Geophys. Res. Lett., 36(8), 4–

607   6, doi:10.1029/2009GL037810, 2009.

608   Erel, Y., Dayan, U., Rabi, R., Rudich, Y. and Stein, M.: Trans boundary transport of pollutants by

609   atmospheric mineral dust, Environ. Sci. Technol., 40(9), 2996–3005, doi:10.1021/es051502l, 2006.

610   Fyfe, J. C., Merryfield, W. J., Kharin, V., Boer, G. J., Lee, W. S. and Von Salzen, K.: Skillful predictions

611   of decadal trends in global mean surface temperature, Geophys. Res. Lett., 38(22), 1–5,

612   doi:10.1029/2011GL049508, 2011.

613   Fyfe, J. C., Gillett, N. P. and Zwiers, F. W.: Overestimated global warming over the past 20 years, Nat.

614   Clim. Chang., 3(9), 767–769, doi:10.1038/nclimate1972, 2013.

615   Gelaro, R., McCarty, W., Suárez, M. J., Todling, R., Molod, A., Takacs, L., Randles, C. A., Darmenov,

616   A., Bosilovich, M. G., Reichle, R., Wargan, K., Coy, L., Cullather, R., Draper, C., Akella, S., Buchard,

617   V., Conaty, A., da Silva, A. M., Gu, W., Kim, G. K., Koster, R., Lucchesi, R., Merkova, D., Nielsen,

618   J. E., Partyka, G., Pawson, S., Putman, W., Rienecker, M., Schubert, S. D., Sienkiewicz, M. and Zhao,

619   B.: The modern-era retrospective analysis for research and applications, version 2 (MERRA-2), J.

620   Clim., 30(14), 5419–5454, doi:10.1175/JCLI-D-16-0758.1, 2017.

621   Graham, N. E.: Decadal-scale climate variability in the tropical and North Pacific during the 1970s and

622   1980s: observations and model results, Clim. Dyn., 10(3), 135–162, doi:10.1007/BF00210626, 1994.

623   Guo, H., Wang, X. and Gao, Z.: Uncertain linear regression model and its application, J. Intell. Manuf.,

624   28(3), 559–564, doi:10.1007/s10845-014-1022-4, 2017.

625   He, L., Lin, A., Chen, X., Zhou, H., Zhou, Z. and He, P.: Assessment of MERRA-2 Surface PM2.5 over

626   the Yangtze River Basin: Ground-based verification, spatiotemporal distribution and meteorological

627 dependence, Remote Sens., 11(4), 460, doi:10.3390/rs11040460, 2019.

628 He, S. and Wang, H.: Oscillating relationship between the East Asian Winter Monsoon and ENSO, J.

629 Clim., 26(24), 9819–9838, doi:10.1175/JCLI-D-13-00174.1, 2013.

630 Hirahara, S., Ishii, M. and Fukuda, Y.: Centennial-scale sea surface temperature analysis and its

631 uncertainty, J. Clim., 27(1), 57–75, doi:10.1175/JCLI-D-12-00837.1, 2014.

632 Hu, S. and Fedorov, A. V.: The extreme El Niño of 2015–2016 and the end of global warming hiatus,

633 Geophys. Res. Lett., 44(8), 3816–3824, doi:10.1002/2017GL072908, 2017.

634 Huang, X., Zhou, T., Turner, A., Dai, A., Chen, X., Clark, R., Jiang, J., Man, W., Murphy, J., Rostron,

635 J., Wu, B., Zhang, L., Zhang, W. and Zou, L.: The recent decline and recovery of Indian summer

636 monsoon rainfall: Relative roles of external forcing and internal variability, J. Clim., 33(12), 5035–

637 5060, doi:10.1175/JCLI-D-19-0833.1, 2020.

638 Jin, Q. and Wang, C.: The greening of Northwest Indian subcontinent and reduction of dust abundance

639 resulting from Indian summer monsoon revival, Sci. Rep., 8(1), 1–9, doi:10.1038/s41598-018-

640 23055-5, 2018.

641 Jin, Q., Wei, J., Pu, B., Yang, Z. L. and Parajuli, S. P.: High Summertime Aerosol Loadings Over the

642 Arabian Sea and Their Transport Pathways, J. Geophys. Res. Atmos., 123(18), 10,568-10,590,

643 doi:10.1029/2018JD028588, 2018.

644 Kaiser, J. and Granmar, M.: Mounting Evidence Indicts Fine-Particle Pollution, Science (80-.).,

645 307(5717), 1858–1861, 2005.

646 Kinter, I. L., Miyakoda, K. and Yang, S.: Recent change in the connection from the Asian monsoon to

647 ENSO, J. Clim., 15(10), 1203–1215, doi:10.1175/1520-0442(2002)015<1203:RCITCF>2.0.CO;2,

648 2002.

649 Kosaka, Y. and Xie, S. P.: Recent global-warming hiatus tied to equatorial Pacific surface cooling, Nature,

650 501(7467), 403–407, doi:10.1038/nature12534, 2013.

651 Krishnamurthy, L. and Krishnamurthy, V.: Influence of PDO on South Asian summer monsoon and

652 monsoon-ENSO relation, Clim. Dyn., 42(9–10), 2397–2410, doi:10.1007/s00382-013-1856-z, 2014.

653 Krishnamurthy, V. and Kirtman, B. P.: Variability of the Indian Ocean: Relation to monsoon and ENSO,

654 Q. J. R. Meteorol. Soc., 129(590), 1623–1646, doi:10.1256/qj.01.166, 2003.

Kucharski, F., Bracco, A., Yoo, J. H. and Molteni, F.: Low-frequency variability of the Indian monsoon-ENSO relationship and the tropical Atlantic: The "weakening" of the 1980s and 1990s, J. Clim., 20(16), 4255–4266, doi:10.1175/JCLI4254.1, 2007.

Kug, J. S., An, S. Il, Jin, F. F. and Kang, I. S.: Preconditions for El Niño and La Niña onsets and their relation to the Indian Ocean, Geophys. Res. Lett., 32(5), 1–5, doi:10.1029/2004GL021674, 2005.

Kumar, K. K., Rajagopalan, B. and Cane, M. A.: On the weakening relationship between the indian monsoon and ENSO, Science (80-.)., 284(5423), 2156–2159, doi:10.1126/science.284.5423.2156, 1999.

Lakshmi, N. B., Nair, V. S. and Suresh Babu, S.: Vertical structure of aerosols and mineral dust over the Bay of Bengal from multisatellite observations, J. Geophys. Res. Atmos., 122(23), 12,845-12,861, doi:10.1002/2017JD027643, 2017.

Lakshmi, N. B., Babu, S. S. and Nair, V. S.: Recent Regime Shifts in Mineral Dust Trends over South Asia from Long-Term CALIPSO Observations, IEEE Trans. Geosci. Remote Sens., 57(7), 4485–4489, doi:10.1109/TGRS.2019.2891338, 2019.

Lee, Y. G., Kim, J., Ho, C. H., An, S. Il, Cho, H. K., Mao, R., Tian, B., Wu, D., Lee, J. N., Kalashnikova, O., Choi, Y. and Yeh, S. W.: The effects of ENSO under negative AO phase on spring dust activity over northern China: An observational investigation, Int. J. Climatol., 35(6), 935–947, doi:10.1002/joc.4028, 2015.

Li, T., Zhang, Y., Lu, E. and Wang, D.: Relative role of dynamic and thermodynamic processes in the development of the Indian Ocean dipole: An OGCM diagnosis, Geophys. Res. Lett., 29(23), doi:10.1029/2002GL015789, 2002.

Liu, J., Wu, D., Liu, G., Mao, R., Chen, S., Ji, M., Fu, P., Sun, Y., Pan, X., Jin, H., Zhou, Y. and Wang, X.: Impact of Arctic amplification on declining spring dust events in East Asia, Clim. Dyn., 54(3–4), 1913–1935, doi:10.1007/s00382-019-05094-4, 2020.

Mahowald, N. M., Kloster, S., Engelstaedter, S., Moore, J. K., Mukhopadhyay, S., McConnell, J. R., Albani, S., Doney, S. C., Bhattacharya, A., Curran, M. A. J., Flanner, M. G., Hoffman, F. M., Lawrence, D. M., Lindsay, K., Mayewski, P. A., Neff, J., Rothenberg, D., Thomas, E., Thornton, P. E. and Zender, C. S.: Observed 20th century desert dust variability: Impact on climateand

biogeochemistry, Atmos. Chem. Phys., 10(22), 10875–10893, doi:10.5194/acp-10-10875-2010, 2010.

Nitta, T. and Yamada, S.: Recent warming of tropical sea surface temperature and its relationship to the Northern Hemisphere circulation, J. Meteorol. Soc. Japan, 67(3), 375–383, doi:10.2151/jmsj1965.67.3_375, 1989.

Osborn, T. J., Jones, P. D., Lister, D. H., Morice, C. P., Simpson, I. R., Winn, J. P., Hogan, E. and Harris, I. C.: Land Surface Air Temperature Variations Across the Globe Updated to 2019: The CRUTEM5 Data Set, J. Geophys. Res. Atmos., 126(2), doi:10.1029/2019JD032352, 2021.

Pallikari, F.: On the false hypothesis of psi-mediated shift of statistical average in tests with random number generators, in The Parapsychological Association Convention 2004, pp. 157–171., 2004.

Parker, D. J., Willetts, P., Birch, C., Turner, A. G., Marsham, J. H., Taylor, C. M., Kolusu, S. and Martin, G. M.: The interaction of moist convection and mid-level dry air in the advance of the onset of the Indian monsoon, Q. J. R. Meteorol. Soc., 142(699), 2256–2272, doi:10.1002/qj.2815, 2016.

Poulsen, O. M., Breum, N. O., Ebbehoj, N., Hansen, A. M., Ivens, U. I., van Lelieveld, D., Malmros, P., Matthiasen, L., Nielsen, B. H. and Nielsen, E. M.: Sorting and recycling of domestic waste. Review of occupational health problems and their possible causes., Sci. Total Environ., 168(1), 33–56, 1995.

Prospero, J. M. and Nees, R. T.: Impact of the North African drought and El Niño on mineral dust in the Barbados trade winds, Nature, 320(6064), 735–738, doi:10.1038/320735a0, 1986.

Randles, C. A., Sliva, A. M. da, Buchard, V., Colarco, P., Armenov, A. and Govindaraju, R.: The MERRA-2 Aerosol Reanalysis, 1980 Onward. Part I: System Description and Data Assimilation Evaluation, J. Clim., 30(17), 6823–6850, doi:10.1175/JCLI-D-16-0609.1, 2017.

Rayner, N. A., Parker, D. E., Horton, E. B., Folland, C. K., Alexander, L. V., Rowell, D. P., Kent, E. C. and Kaplan, A.: Global analyses of sea surface temperature, sea ice, and night marine air temperature since the late nineteenth century, J. Geophys. Res. Atmos., 108(D14), 4407, doi:10.1029/2002jd002670, 2003.

Razakov, R. M. and Kosnazarov, K. A.: Dust and salt transfer from the exposed bed of the Aral Sea and measures to decrease its environmental impact, in The Aral Sea Basin, edited by P. P. Micklin and W. D. Williams, pp. 95–102, Springer, Berlin, Heidelberg., 1996.

711 Richon, C., Dutay, J., Dulac, F. and Wang, R.: Modeling the biogeochemical impact of atmospheric

712   phosphate deposition from desert dust and combustion sources to the Mediterranean Sea,

713   Biogeosciences, 15(8), 2499–2524, doi:10.5194/bg-2017-242, 2018.

714 Rienecker, M. M., Suarez, M. J., Gelaro, R., Todling, R., Bacmeister, J., Liu, E., Bosilovich, M. G.,

715   Schubert, S. D., Takacs, L., Kim, G. K., Bloom, S., Chen, J., Collins, D., Conaty, A., Da Silva, A.,

716   Gu, W., Joiner, J., Koster, R. D., Lucchesi, R., Molod, A., Owens, T., Pawson, S., Pegion, P., Redder,

717   C. R., Reichle, R., Robertson, F. R., Ruddick, A. G., Sienkiewicz, M. and Woollen, J.: MERRA:

718   NASA's modern-era retrospective analysis for research and applications, J. Clim., 24(14), 3624–

719   3648, doi:10.1175/JCLI-D-11-00015.1, 2011.

720 Sabeerali, C. T., Ajayamohan, R. S., Bangalath, H. K. and Chen, N.: Atlantic Zonal Mode: An Emerging

721   Source of Indian Summer Monsoon Variability in a Warming World, Geophys. Res. Lett., 46(8),

722   4460–4467, doi:10.1029/2019GL082379, 2019.

723 Sanchez de la Campa, A., Garcia-Salamanca, A., Solano, J., de la Rosa, J. and Ramos, J.-L.: Chemical

724   and microbiological characterization of atmospheric particulate matter during an intense African dust

725   event in Southern Spain., Environ. Sci. Technol., 47(8), 3630–3638, doi:10.1021/es3051235, 2013.

726 Schulz, M., Prospero, J. M., Baker, A. R., Dentener, F., Ickes, L., Liss, P. S., Mahowald, N. M., Nickovic,

727   S., García-Pando, C. P., Rodríguez, S., Sarin, M., Tegen, I. and Duce, R. A.: Atmospheric Transport

728   and Deposition of Mineral Dust to the Ocean: Implications for Research Needs, Environ. Sci.

729   Technol., 46(19), 10390–10404, doi:10.1021/es300073u, 2012.

730 Singh, R. P., Prasad, A. K., Kayetha, V. K. and Kafatos, M.: Enhancement of oceanic parameters

731   associated with dust storms using satellite data, J. Geophys. Res., 113, C11008,

732   doi:10.1029/2008JC004815, 2008.

733 Srivastava, G., Chakraborty, A. and Nanjundiah, R. S.: Multidecadal see-saw of the impact of ENSO on

734   Indian and West African summer monsoon rainfall, Clim. Dyn., 52(11), 6633–6649,

735   doi:10.1007/s00382-018-4535-2, 2019.

736 Storch, H. von and Zwiers, F. W.: Statistical Analysis in Climate Research, Cambridge University Press,

737   Cambridge., 1999.

738 Tokinaga, H., Richter, I. and Kosaka, Y.: ENSO Influence on the Atlantic Niño, Revisited: Multi-Year

739   versus Single-Year ENSO Events, J. Clim., 32(14), 4585–4600, 2019.

740   Trenberth, K. E. and Hurrell, J. W.: Decadal atmosphere-ocean variations in the Pacific, Clim. Dyn., 9(6),

741   303–319, doi:10.1007/BF00204745, 1994.

742   Trenberth, K. E., Dai, A., Van Der Schrier, G., Jones, P. D., Barichivich, J., Briffa, K. R. and Sheffield,

743   J.: Global warming and changes in drought, Nat. Clim. Chang., 4(1), 17–22,

744   doi:10.1038/nclimate2067, 2014.

745   Veselovskii, I., Goloub, P., Podvin, T., Tanre, D., Da Silva, A., Colarco, P., Castellanos, P., Korenskiy,

746   M., Hu, Q., Whiteman, D. N., Pérez-Ramírez, D., Augustin, P., Fourmentin, M. and Kolgotin, A.:

747   Characterization of smoke and dust episode over West Africa: Comparison of MERRA-2 modeling

748   with multiwavelength Mie-Raman lidar observations, Atmos. Meas. Tech., 11(2), 949–969,

749   doi:10.5194/amt-11-949-2018, 2018.

750   Wang, B., Wu, R. and Li, T.: Atmosphere-warm ocean interaction and its impacts on Asian-Australian

751   monsoon variation, J. Clim., 16(8), 1195–1211, doi:10.1175/1520-

752   0442(2003)16<1195:AOIAII>2.0.CO;2, 2003.

753   Wang, L., Chen, W. and Huang, R.: Interdecadal modulation of PDO on the impact of ENSO on the east

754   Asian winter monsoon, Geophys. Res. Lett., 35(20), doi:10.1029/2008GL035287, 2008.

755   Wang, S., Huang, J., He, Y. and Guan, Y.: Combined effects of the Pacific Decadal Oscillation and El

756   Niño-Southern Oscillation on Global Land Dry-Wet Changes, Sci. Rep., 4, 6651,

757   doi:10.1038/srep06651, 2014.

758   Watanabe, M. and Jin, F. F.: Role of Indian Ocean warming in the development of Philippine Sea

759   anticyclone during ENSO, Geophys. Res. Lett., 29(10), 1161–1164, doi:10.1029/2001gl014318,

760   2002.

761   Watanabe, M., Shiogama, H., Tatebe, H., Hayashi, M., Ishii, M. and Kimoto, M.: Contribution of natural

762   decadal variability to global warming acceleration and hiatus, Nat. Clim. Chang., 4(10), 893–897,

763   doi:10.1038/nclimate2355, 2014.

764   Weare, B. C., Navato, A. R. and Newell, R. E.: Empirical orthogonal analysis of Pacific sea surface

765   temperatures, J. Phys. Oceanogr., 6(5), 671–678, 1976.

766   Weng, H., Ashok, K., Behera, S. K., Rao, S. A. and Yamagata, T.: Impacts of recent El Niño Modoki on

767 dry/wet conditions in the Pacific rim during boreal summer, Clim. Dyn., 29(2–3), 113–129,

768 doi:10.1007/s00382-007-0234-0, 2007.

769 Wu, R. and Kirtman, B. P.: Understanding the impacts of the Indian ocean on ENSO variability in a

770 coupled GCM, J. Clim., 17(20), 4019–4031, doi:10.1175/1520-

771 0442(2004)017<4019:UTIOTI>2.0.CO;2, 2004.

772 Xi, X. and Sokolik, I. N.: Dust interannual variability and trend in Central Asia from 2000 to 2014 and

773 their climatic linkages, J. Geophys. Res. Atmos., 120(23), 12175–12191, doi:10.1038/175238c0,

774 2016.

775 Yang, S. and Jiang, X.: Prediction of Eastern and Central Pacific ENSO Events and Their Impacts on

776 East Asian Climate by the NCEP Climate Forecast System, J. Clim., 27(12), 4451–4472,

777 doi:10.1175/JCLI-D-13-00471.1, 2014.

778 Yang, X. and Huang, P.: Restored relationship between ENSO and Indian summer monsoon rainfall

779 around 1999/2000, Innov., 2(2), 100102, doi:10.1016/j.xinn.2021.100102, 2021.

780 Yu, J.-Y., Mechoso, C. R., McWilliams, J. C. and Arakawa, A.: Impacts of the Indian Ocean on the

781 ENSO cycle, Geophys. Res. Lett., 29(8), 1204, 2002.

782 Yu, J. and Kao, H.: Decadal changes of ENSO persistence barrier in SST and ocean heat content indices :

783 1958 – 2001, J. Geophys. Res., 112(D13), 1–10, doi:10.1029/2006JD007654, 2007.

784 Yu, Y., Notaro, M., Liu, Z., Wang, F., Alkolibi, F., Fadda, E. and Bakhrjy, F.: Climatic controls on the

785 interannual to decadal variability in Saudi Arabian dust activity: Toward the development of a

786 seasonal dust prediction model, J. Geophys. Res. Atmos., 120(5), 1739–1758,

787 doi:10.1002/jgrc.20224, 2015.

788 Yuan, Y. and Yang, S.: Impacts of Different Types of El Niño on the East Asian Climate: Focus on

789 ENSO Cycles, J. Clim., 25(21), 7702–7722, 2012.

790